J Solid State Electrochem (2009) 13:321–332
DOI 10.1007/s10008-008-0550-2

ORIGINAL PAPER

The effects of electropolishing on the nanochannel ordering of the porous anodic alumina prepared in oxalic acid

Abdur Rauf · Mazhar Mehmood · Muhammad Asim Rasheed · Muhammad Aslam

Received: 22 December 2006 / Revised: 6 March 2008 / Accepted: 6 March 2008 / Published online: 24 April 2008

Abstract A series of porous anodic alumina has been prepared by anodizing aluminum surface in 0.3 M oxalic acid at different voltages. Prior to anodizing, the surface was pretreated in two different electropolishing electrolytes. One was Brytal solution (15% Na_2CO_3 and 5% Na_3PO_4) at 80 °C in which the electropolishing was performed at 2 V. This resulted in about 100–150 nm apart random features of 4–5 nm height. The other was the commonly employed perchloric acid–alcohol solution (1:4 ratio by volume), in which the electropolishing was performed at 20 V. The resulting surface comprised nanostripes of 1–2 nm amplitude with a wavelength of about 50 nm. The former pretreatment proved better for self-ordering of the pores at the anodizing voltage of 50–60 V, while the latter pretreatment was found better at the anodizing voltage of 40 V. The improved pore ordering at a given voltage was attributed to the higher pore density as associated with greater repulsive interactions among the pores.

Introduction

Nanostructured materials exhibit interesting properties in a wide range of spectrum including catalytic activity [1], corrosion resistance [2], optical properties [3] and magnetic properties [4]. One of the important nanostructures which has tremendous applications in nanotechnology is self-organized hexagonally ordered anodic alumina [5]. Anodic oxidation of aluminum can result in the formation of compact barrier oxide [6–9], porous oxide [10–21], or dissolution or electropolishing of aluminum [22, 23], depending on the electrolyte, temperature, and applied voltage. An explosion of porous alumina research was ignited once the capability of producing a nanohole array with excellent regularity was established by Masuda et al. [11]. Self-organization of anodic alumina has been mostly achieved by the two-step anodizing the aluminum surface after electropolishing in perchloric acid–alcohol solution. The best self-ordering voltages have been found to be 25, 40, and 195 V when anodizing is performed in sulfuric, oxalic, and phosphoric acids, respectively, within a range of concentration and temperature of the electrolytes [12–21]. There is a specific cell size or lattice parameter of the hexagonal order corresponding to the anodizing voltage [11–13, 21]. The hexagonality is lost, or its quality deteriorates as the anodizing voltage deviates from the optimum one in a given electrolyte [12–14].

With a narrow distribution of pore diameters and interpore distances of the self-organized anodic alumina, it could be used in a variety of applications, particularly as a template to form nanowires, nanotubes, nanodots, and composites for catalysis, emitters, rechargeable batteries, magnetic storage devices, etc [24–28]. The superlattice of pores and nanowires in anodic alumina has also been found extremely useful to exploit and study magnetic interactions, dielectric properties, and optical interference [5, 29, 30]. The applications are further being extended due to the possibilities of forming multiple layers of the anodic alumina. For instance, two or more layers with different diameters can be formed over each other, giving Y-type nanopores at the joint (Rauf A, Yuan ZH, Mehmood M (to be submitted))[31, 32]. Formation of two porous layers with same diameter separated by a barrier layer has also been explored by anodic oxidation of aluminum sheet from both sides [33].

A. Rauf · M. Mehmood (✉) · M. Asim Rasheed · M. Aslam
National Center for Nanotechnology
and Department of Chemical and Materials Engineering,
Pakistan Institute of Engineering and Applied Science,
Islamabad 45650, Pakistan
e-mail: mazhar@pieas.edu.pk

Table 1 The details of the experimental parameters for the preparation of anodic alumina

Experimental sets	Electropolishing details	Electrolyte and temperature	Anodizing conditions (V)	Samples sets
1	Perchloric acid and alcohol (4:1 ratio by volumes) solution (stirring) at 20 V and temperature below 10 °C	0.3 M oxalic acid at 1±1 °C	40 50 60 70	Set A
2	Brytal solution (Stirring) at 2 V and temperature of 80 °C	0.3 M oxalic acid at 1±1 °C	30 40 50 60 70	Set B

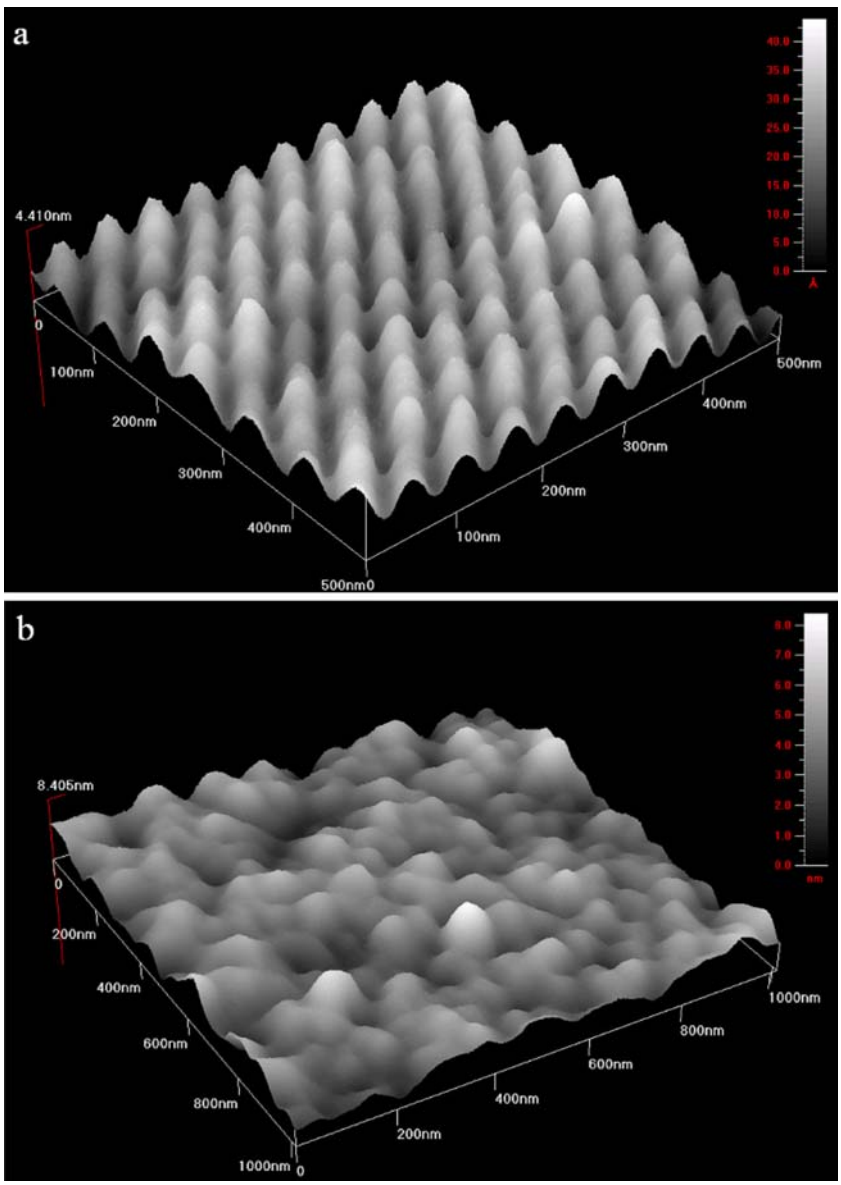

Fig. 1 Typical AFM images of aluminum surfaces after electropolishing in **a** perchloric acid–alcohol solution at 20 V (Set A) and **b** Brytal solution at 2 V (Set B)

Pretexturing the surfaces by different physical techniques has been found to widen the range of ordering voltages in a given electrolyte [14, 18, 34–36]. This plays its role at the nucleation stage of pore formation as the pores are formed directly on the troughs of pretextured surfaces. This has been useful to extend the cell sizes for long range ordering, however, with limited aspect ratio [18]. This suggests that the nanoscale surface morphology or nanotexture of the aluminum surface before anodizing is important for ordering at a given voltage [18, 35, 36].

Atomic force microscopic (AFM) studies have revealed that electropolishing of aluminum results in a variety of nanoscale surface morphologies, including self-patterned regular pits and stripes [37–39]. In addition, the nanomorphology strongly depends on the electropolishing conditions [37] and chemistry of the electrolyte [23] used for the electropolishing.

In most of the cases for self-organized anodic alumina, the electropolishing of aluminum has been carried out in the solution containing perchloric acid, presuming it to be the most appropriate electropolishing solution due to its ability to provide extraordinary smooth surfaces. However, variation in nanoscale features, depending on the electropolishing treatment or electrolyte, may affect the pore ordering similar to the other pretexturing treatments, which change the nucleation density and, thus, influence the interpore interactions. This may influence the ordering phenomenon and, thus, the quality of ordering. This aspect has been focused upon in the present work.

Experimental

$C_2H_2O_4.2H_2O$ (Riedel, 97.5%), Na_2CO_3 (Panreac, 99.5%), Na_3PO_4 $12H_2O$ (Riedel, 98%), $CrO_3.2H_2O$ (Merk, 99%), and H_3PO_4 (BDH, 98%) were purchased from commercial resources and used without further processing. High purity aluminum sheet (99.99%, 0.5 mm thick) was used as a starting material. The samples were heat treated at 500 °C for 5 days and degreased ultrasonically in acetone for about 15 min. The long heat treatment time was meant for ensuring a significant crystal growth. Two sets of experiments were performed as shown in Table 1. For Set A, the samples were electropolished in perchloric acid–alcohol (20%$HClO_4$ and 80%C_2H_5OH by volume) solution at 20 V with the bath temperature below 10 °C. While for Set B, the samples were electropolished in Brytal solution (15% Na_2CO_3 and 5% Na_3PO_4) at 80 °C and 2 V. For anodizing, the electrolyte was 0.3 M oxalic acid. Temperature during anodizing was maintained at 1 °C (±1 °C), unless mentioned otherwise in the results. The anodizing was performed in two steps, namely first anodizing and second anodizing. First anodizing of different samples was carried out at 30 to 70 V for 12 to 3 h; the higher the voltages, the shorter the anodizing time. The anodic alumina was, then, dissolved in a solution containing 0.2 M CrO_3 H_2O and 0.4 M H_3PO_4 at 80 °C for more than 3 h. Then, second anodizing was performed under the same conditions as that of the first anodizing for several hours.

Electropolishing and anodizing were performed using Stabilized Power Supply (FARNELL, TSV70 MK.2) with two electrode configuration; the counter electrode being a platinum plate. The current vs. time (*I-t*) curves were obtained using Function Generator (AMEL Mod-7800-Interface) and Potentiostat or Galvanostat (AMEL Model 2053) in combination with a Programmable Power Supply (GW INSTEK, PSP-603). The samples were characterized using Scanning Electron Microscope (SEM; LEO-441-I), Field Emission SEM (FESEM, LEO 1550), and AFM (QUESANT (Ambios) USPM).

Results

Electropolishing

Figure 1a and b show typical AFM images of aluminum surfaces after electropolishing in perchloric acid–alcohol solution at 20 V (Set A) and in Brytal solution at 2 V (Set B), respectively. (From here onwards, the samples prepared by electropolishing in Perchloric acid–alcohol solution will be called as Set A samples and the samples prepared by electropolishing in Brytal solution will be called as Set B samples.) An ordered structure composed of typical nanostripes is formed on the surface of the Set A samples, as

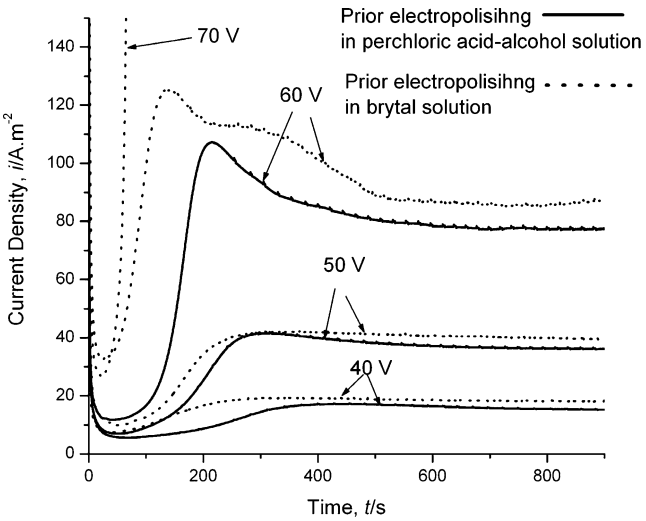

Fig. 2 Typical current vs. time (*I-t*) curves during first anodizing in 0.3 M oxalic acid at 1 °C, as a function of anodizing voltage and prior electropolishing conditions

typically shown in Fig. 1a. The peak-to-peak distance is of the order of 50 nm, while the trough depth is of the order of 2 nm. On the other hand, the surface of Set B samples exhibits a cellular structure composed of randomly located nanopits or depressions with an average distance of more than 100 nm, as typically shown in Fig. 1b. The average depth of these depressions is of the order of 5 nm that is greater than the trough depth of the nanostripes observed in Set A samples.

First anodizing

After electropolishing, the samples were anodized in 0.3 M oxalic acid at different voltages. Figure 2 shows typical *I-t* curves during first anodizing as a function of anodizing voltage and prior electropolishing conditions. The shape of the curves is typical for anodizing in oxalic acid, whereas initial decrease in current corresponds to the formation of barrier oxide, and then, a rise is associated with localized thinning of the barrier layer that ultimately leads to the formation of vertical pores. This results in a typical two-layer structure of anodic alumina comprising a continuously growing porous layer lying over a barrier layer [15]. The time required for rise in current, after following its minimum value, is clearly longer in case of the Set A samples in comparison with the Set B samples. This seems to be associated with the difference in smoothness and nanoscopic features (Fig. 1) of the surfaces; the relatively rougher features or deeper etch pits on the surface of the Set B samples may be responsible for a relatively rapid

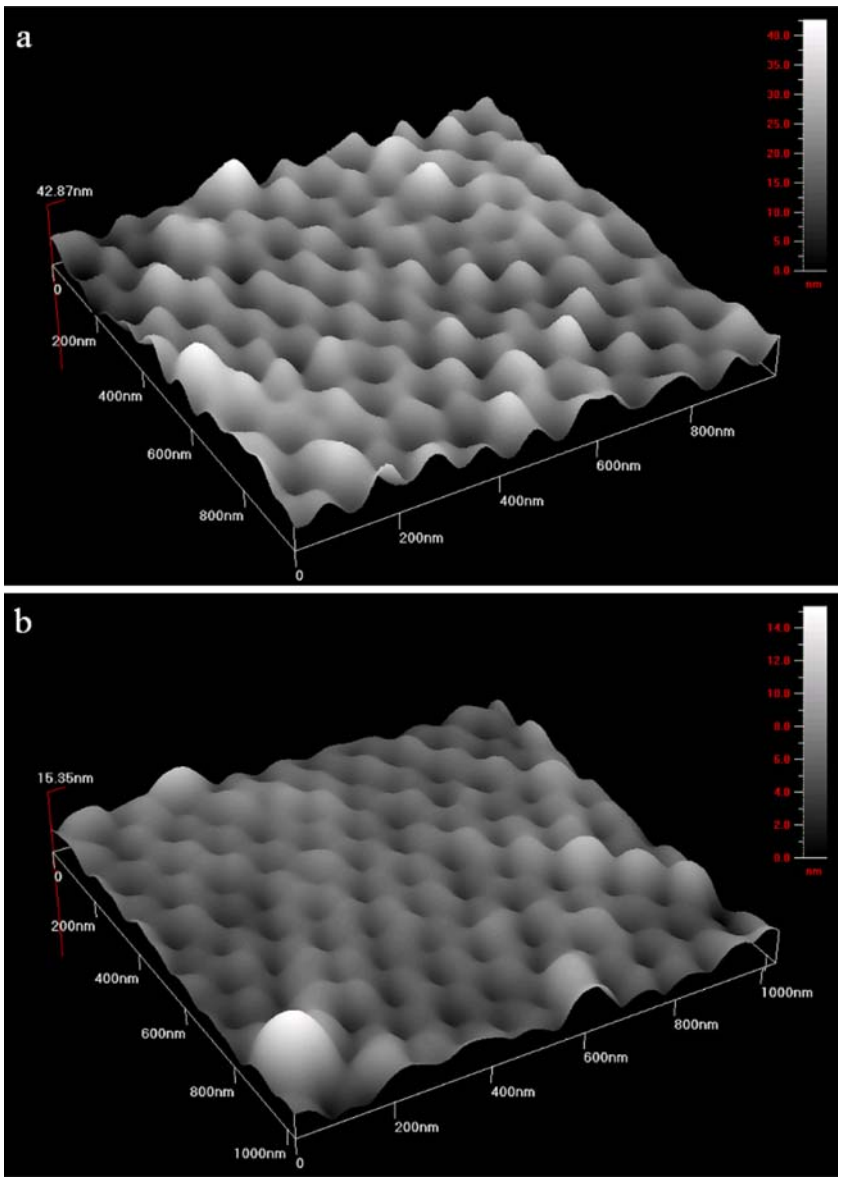

Fig. 3 Typical AFM images after first anodizing and subsequent dissolution to reveal the underlying aluminum surface; the anodizing conditions were: **a** 40 V for 12 min, Set A; **b** 40 V for 7 h, Set A; **c** 50 V for 3 h, Set A; **d** 50 V for 3 h, Set B

Fig. 3 (continued)

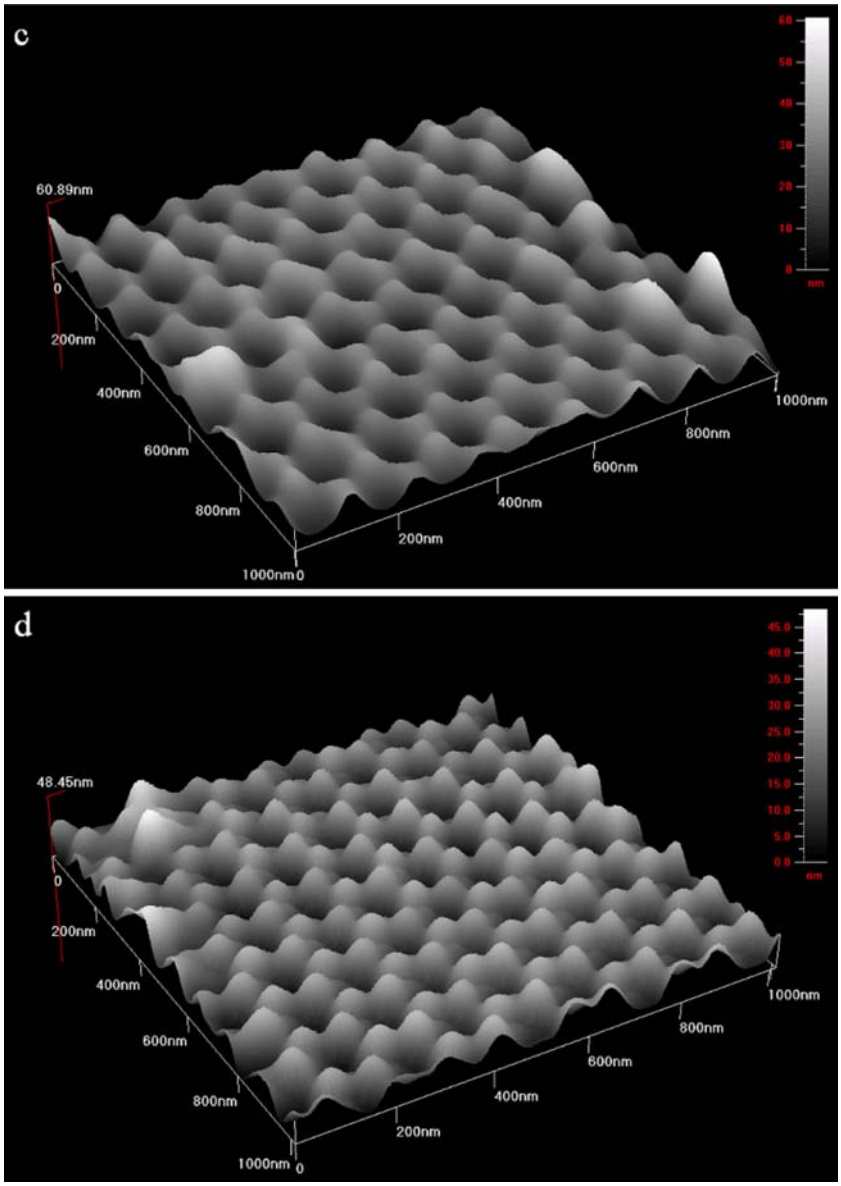

localized thinning of the barrier layer resulting in an earlier rise in current. The anodizing current density remains higher in case of Set B samples even after 900 s (15 min). This may be due to a comparatively higher pore density resulting from ease in their nucleation. Although not shown here, the current density of the Set B samples remain higher after long time anodizing, except for 40 V at which the current density exhibited by the Set A samples exceeds that of the Set B samples after about 2–3 h anodizing.

Figure 3a and b shows typical AFM images of aluminum surfaces of Set A samples after first anodizing at 40 V for 12 min and 7 h, respectively, followed by dissolution of oxide. The dissolution of oxide was carried out in order to reveal the order, if any, at the end of first anodizing for a specified time interval. The several nanometers deep nano-pits created by this treatment correspond to the protrusions formed by oxide at the pore tips. Accordingly, these pits indicate the locations of pore tips at the end of first anodizing. In spite of the fact that a regular pattern of nanostripes existed after electropolishing, an ordered pattern of the pores is not seen after 12 min anodizing as revealed by Fig. 3a. This indicates that a regular patterned surface obtained by this popular electropolishing treatment (Set A) has not been responsible for nucleating any ordered domains. Accordingly, the hexagonal arrangement (Fig. 3b) must owe to the spontaneous adjustment of the pores during their growth. As shown in Fig. 3c and d, the hexagonal order has also been obtained successfully after long time anodizing at 50 V both in case of Set A (Fig. 3c) and Set B (Fig. 3d).

AFM images were subjected to Fast Fourier Transform (FFT) analysis. In order to cover larger number of domains with varying ordering orientations and for improved statistics, larger AFM images of about 5×5 micron size were selected for this analysis. The FFT images obtained by this analysis are shown in Fig. 4. The formation of regular pattern and periodicity (Fig. 3b) has resulted in the formation of a ring (Fig. 4b) in case of the sample anodized at 40 V for long time, and a diffused FFT image is obtained after 12 min anodizing (Fig. 4a) in agreement with the AFM image of the same sample (Fig. 3a). A more significant aspect is the formation of sharper rings or spots in Fig. 4d, as compared with Fig. 4c, suggesting that a relatively better order or periodicity can be achieved at 50 V if prior electropolishing is performed in Brytal solution (Set B) instead of Perchloric acid–alcohol solution (Set A).

Second anodizing

The samples after first anodizing and subsequent dissolution of the oxide were subjected to second anodizing. The *I-t* curves obtained during the second anodizing are shown in Fig. 5. It may be noticed that the minima with a subsequent rise in current appear at an early stage, in comparison with the first anodizing for all the samples (Fig. 2). This seems to be attributable to the deeper nanopits on aluminum surface, as it is clearly evident from

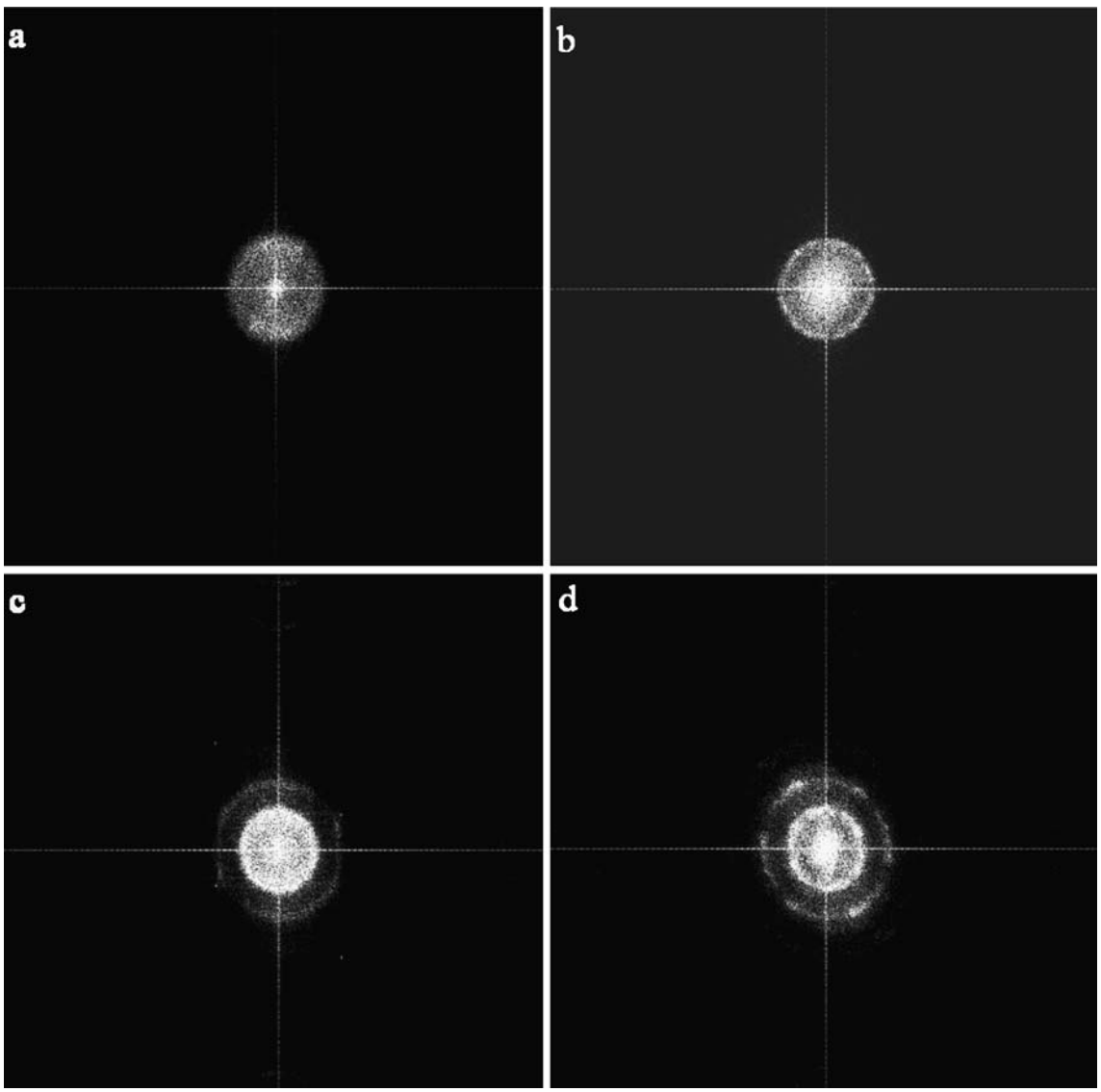

Fig. 4 Fast Fourier Transform images obtained by analysis of the AFM images of 5×5 micron size; the samples were prepared by first anodizing and subsequent dissolution to reveal the underlying aluminum surface; the anodizing conditions were: **a** 40 V for 12 min, Set A; **b** 40 V for 7 h, Set A; **c** 50 V for 3 h, Set A; **d** 50 V for 3 h, Set B

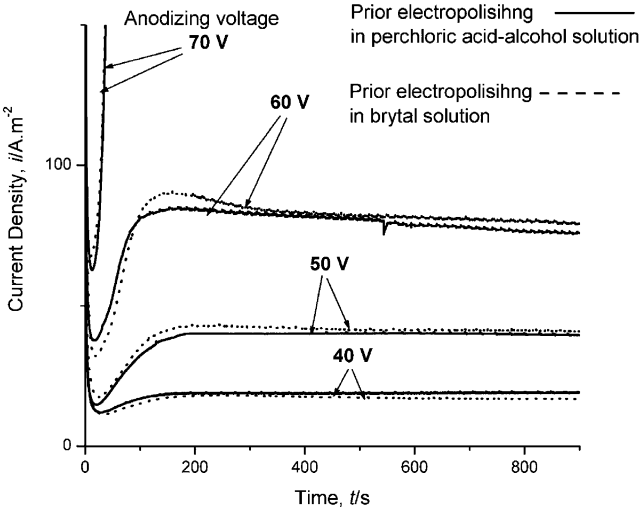

Fig. 5 Typical current vs. time *(I-t)* curves during second anodizing in 0.3 M oxalic acid at about 1 °C, as a function of anodizing voltage and prior electropolishing conditions

comparison between the Figs. 1 and 3. These nanopits must have effectively provided the nucleation sites for the pores during second anodizing. During growth of oxide at anodizing voltage of 50 V and above, the current density is higher in case of the Set B samples in comparison with the Set A samples. On the other hand, the current density is higher in case of Set A sample in comparison with Set B sample when anodizing is performed at 40 V. This suggests a comparatively higher pore density or lower barrier layer thickness in case of Set B sample when the second anodizing was performed at 50 V and above, and vice versa at the anodizing voltage of 40 V.

Figures 6 and 7 show typical SEM images of the top surfaces of the anodic alumina, after second anodizing of the Set A and Set B samples, respectively. Hexagonal ordering is observed at the top surface in case of the samples prepared at 40 and 50 V irrespective of the electropolishing pretreatment. On comparing the second anodizing voltages, the best regular nanohole arrays in the Set A have been observed in the sample prepared at 40 V with substantially larger ordered domains (Fig. 6), which is in agreement with other authors who used perchloric acid–alcohol solution for electropolishing and found 40 V to be the best ordering voltage in oxalic acid [11, 14, 15]. Dissimilar from the Set A samples, the best ordering voltage during second anodizing is observed to be 50 V in case of the Set B samples (Fig. 7). It may also be noticed that the Set B sample anodized at 60 V (Fig. 7c) exhibits mixed regions of ordered domains and disordered regions, i.e., some order still persists, in contrast to Fig. 6c.

The defects in periodicity, as defined by the missing pore sites surrounded by six or five pores (white dots) and the pores surrounded by seven pores, are indicated on Fig. 7b as X, Y, and Z, respectively. The pores with six surrounding pores have not been included in defects even if a true hexagon is not formed, as in the case of samples that do not exhibit hexagonal order. It is quite evident from Figs. 6 and 7 that the defects are mostly located at domain boundaries,

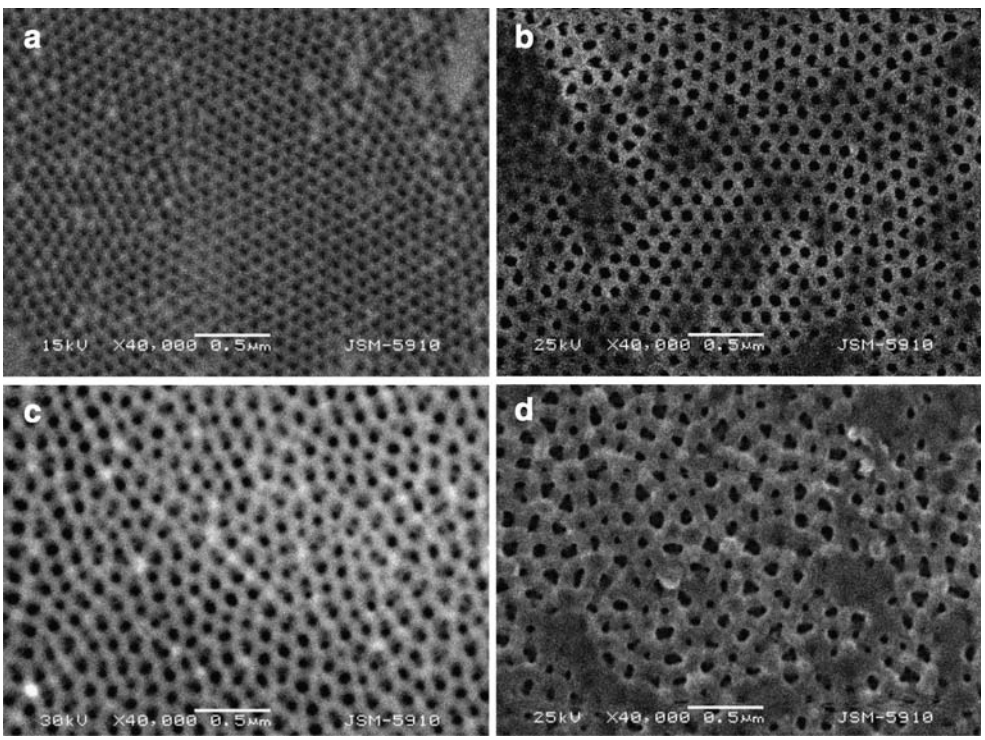

Fig. 6 Typical SEM images of the top surface of the anodic alumina prepared by the two-step anodizing in 0.3 M oxalic acid at 1 °C with prior electropolishing in Perchloric acid–alcohol solution (Set A); the anodizing voltages was **a** 40 V, **b** 50 V, **c** 60 V, and **d** 70 V

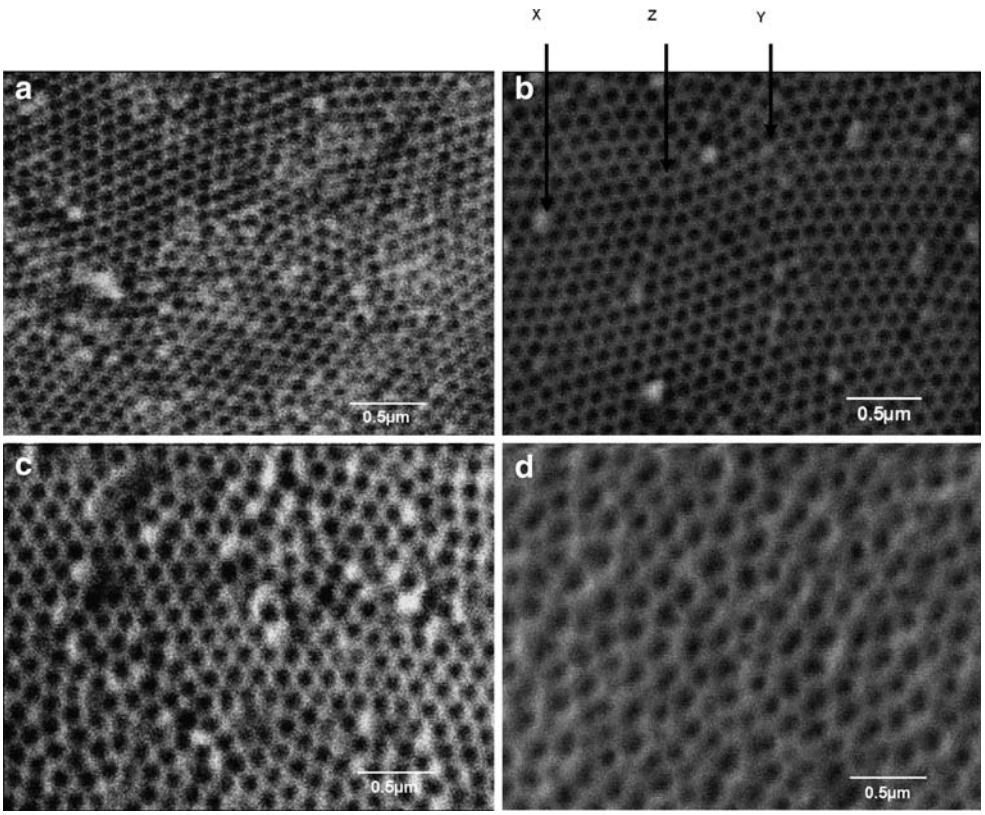

Fig. 7 Typical SEM images of the top surface of the anodic alumina prepared by the two-step anodizing in 0.3 M oxalic acid at 1 °C with prior electropolishing in Brytal solution (Set B); the anodizing voltages were **a** 40 V, **b** 50 V, **c** 60 V, and **d** 70 V

which are at the junctions of differently orientated ordered nanohole-arrayed domains, in case of self-ordering. Quantitatively, it has been shown in Fig. 8 that the percent defects vary with the anodizing voltages. For the samples electropolished in Brytal solution (Set B), the minimum is found at 50 V. More specifically, the sample anodized at 50 V proves to be better in ordering than 40 V in case of Set B samples, as observed at a different temperature, i.e., 10 °C. By contrast, the sample anodized at 40 V exhibits better ordering as compared to the higher anodizing voltage in case of Set A samples.

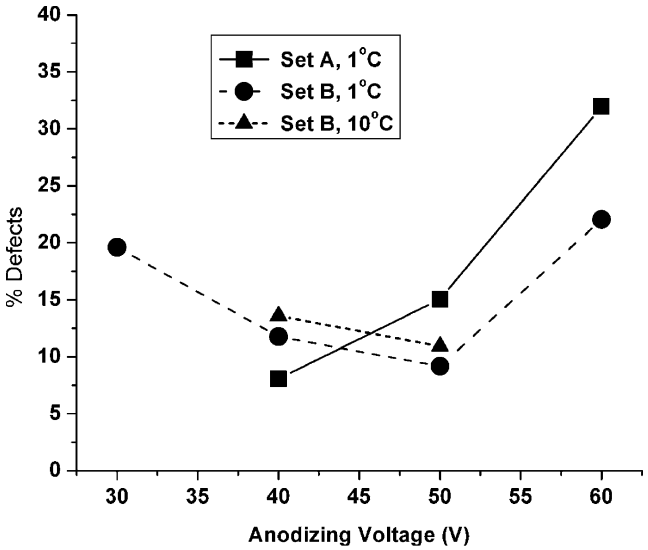

Fig. 8 Variation of percent defects (defined as hundred times the total number of defects divided by the total number of pores of the SEM image) with the anodizing voltage and prior electropolishing

Further investigation on hexagonality was performed by Fast Fourier Transforms of the SEM images of the anodic films formed by second anodizing. A typical FFT image for the Set B sample anodized at 50 V is shown in Fig. 9a. The intensity vs. radial distance from the center of the FFT image as a function of anodizing voltage has been shown in Fig. 9b. It may be noticed that the peak width, as usually determined in terms of Full Width at Half Maximum (FWHM), varies with the anodizing conditions. The FWHM or peak position (Fig. 9c), which is a measure of the scatter of the interpore distance (or wave vectors) with respect to their mean value, exhibits minimum at 50 V indicating a more uniform interpore spacing with respect to the other anodizing voltages for Set B samples. This confirms the visual impression obtained from the corresponding SEM images (Fig. 7).

The peak position (r_p) in the FFT curve (Fig. 9b) should be proportional to the wave vector of periodic wave formed by the pores. Hence, its reciprocal ($1/r_p$) should be proportional to the interpore distance or the cell size. On the other hand, the anodizing voltage may be considered proportional to the barrier layer thickness [40]. This implies

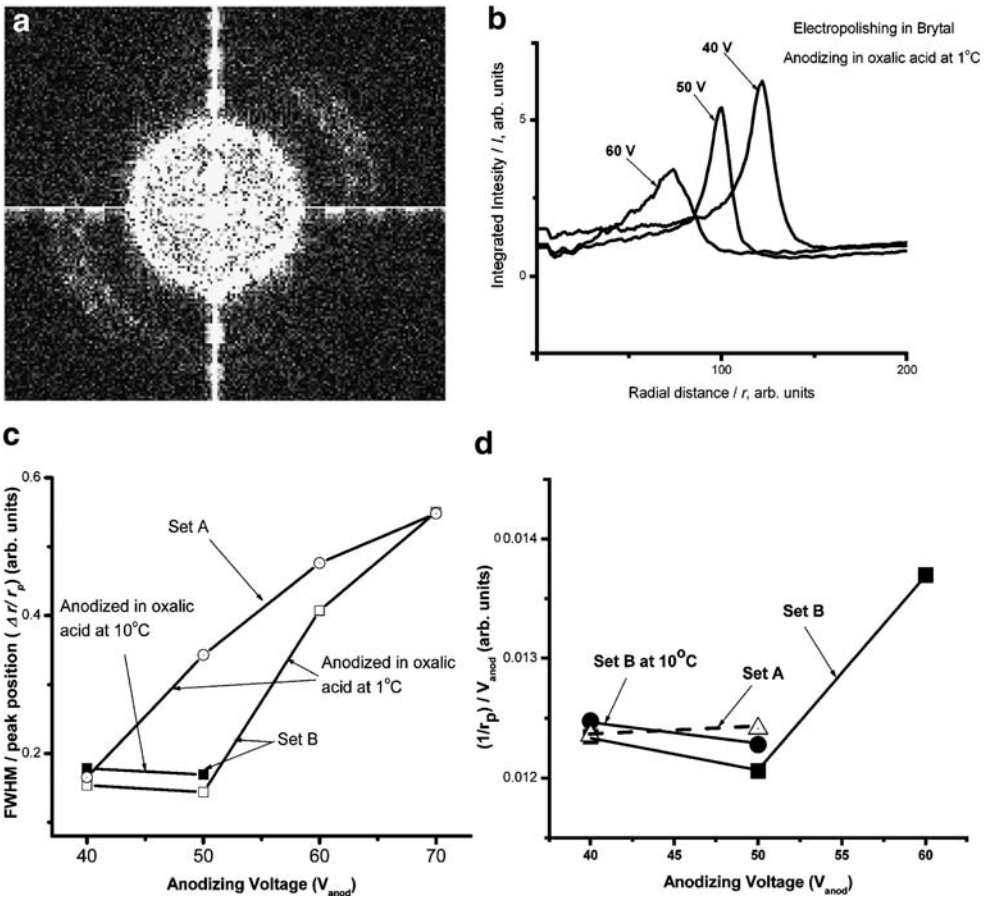

Fig. 9 Results of FFT analysis of SEM images of about 5×5 micron size. The samples were prepared by second anodizing; **a** a typical FFT image, 50 V anodizing, Set B, **b** Integrated intensity of the FFT image, as a function of radial distance (a measure of wave vector) from center (zero wave vector position), Set B, **c** FWHM or peak position vs. anodizing voltage, Set B, **d** $(1/rp)/V_{anod}$ as a function of anodizing voltage

that $(1/r_p)/V_{anod}$ should be proportional to the ratio of cell size to barrier layer thickness, which is considered to be an important parameter for pore ordering [41]. It can be seen in Fig. 9d that the values of $(1/r_p)/V_{anod}$ is lowest at the anodizing voltage of 50 V for the Set B samples, while this is higher for 50 than for 40 V in case of the Set A samples. It may be said that the smaller ratio of the interpore distance (or the wall thickness) to the barrier layer thickness favors the hexagonal ordering by providing the strongest repulsive interactions among the pore tips [42].

Non-ordering voltages

In order to understand the phenomenon at non-ordering voltages, some of the samples were examined at high magnification using FESEM as typically shown in Fig. 10. It may be noticed, by comparing Figs. 10a and 3b, that almost each nanopit leads to the formation of a nanopore in the porous oxide during second anodizing in case of the ordering voltages. By contrast, most of the nanopits present prior to second anodizing lead to the nucleation of two to four pores in case of non-ordering voltages as typically revealed by comparison between Fig. 10b and c. This may be attributable to the irregular shape of the nanopits prior to second anodizing, as formed by first anodizing and subsequent dissolution of the oxide (Fig. 10c).

The cross-sectional FESEM images of the anodic alumina prepared at 40, 50, and 60 V in the Set B are shown in Fig. 11. The pores tend to grow perfectly parallel to each other, maintaining a constant interpore distance in case of the ordering voltage, as shown in Fig. 11a and b. On the other hand, some of the pores cease to grow or undergo branching when the anodizing conditions are not sufficiently suitable for ordering, e.g., anodizing at 60 V, as typically shown in Fig. 11c. The pore branching is in agreement with the formation of more than one pore at a given nanopit (Fig. 10b). Hence, the metal–oxide interface at the pore tip seems to facilitate pore branching during the growth of oxide, possibly due to its irregular shape.

Discussion

It has been shown that best ordering voltage is 40 V when anodizing is performed in 0.3 M oxalic acid after electropolishing in Perchloric acid–alcohol solution, which is in agreement with other researchers [11–13]. This electropolishing resulted in the formation of nanostripes (Fig. 1a).

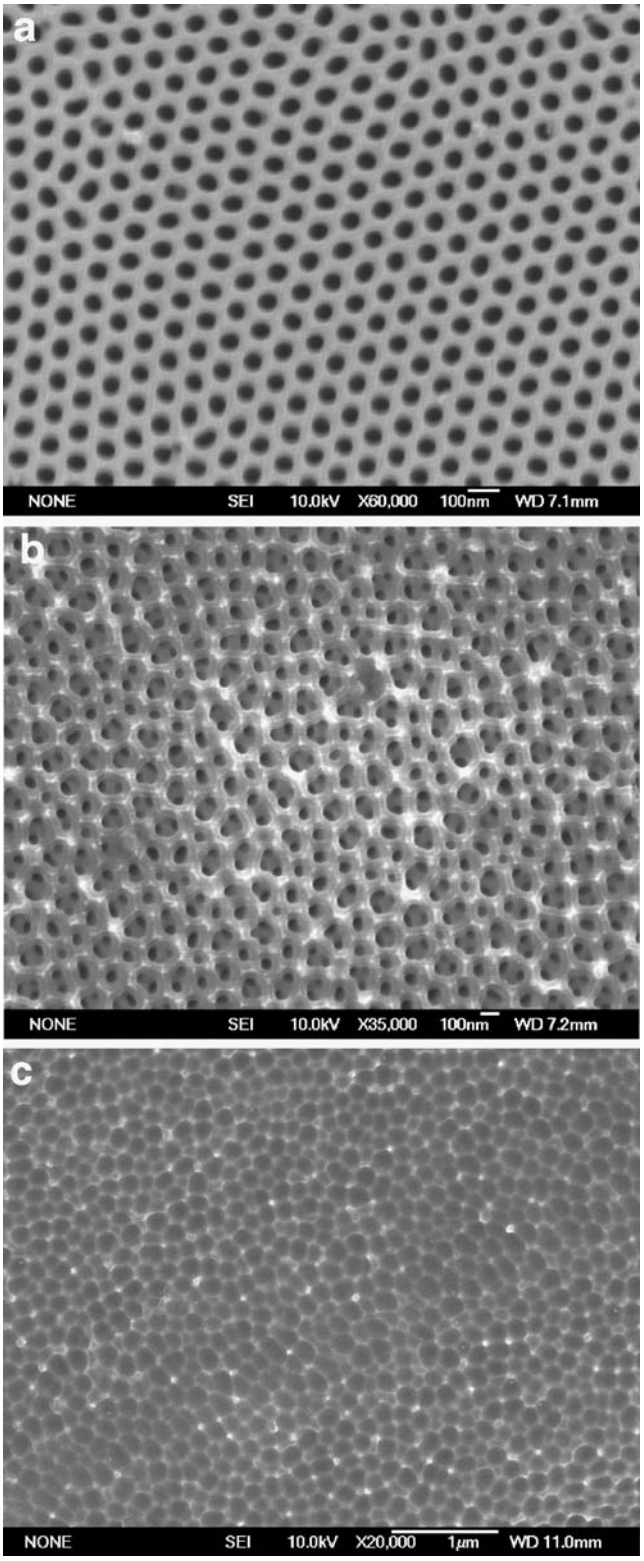

Fig. 10 Typical FESEM obtained for higher resolution, **a** second anodizing at 40 V, Set A; **b** second anodizing at 70 V, Set A; **c** first anodizing at 70 V, followed by dissolution of oxide, the surface prior to second anodizing, Set A

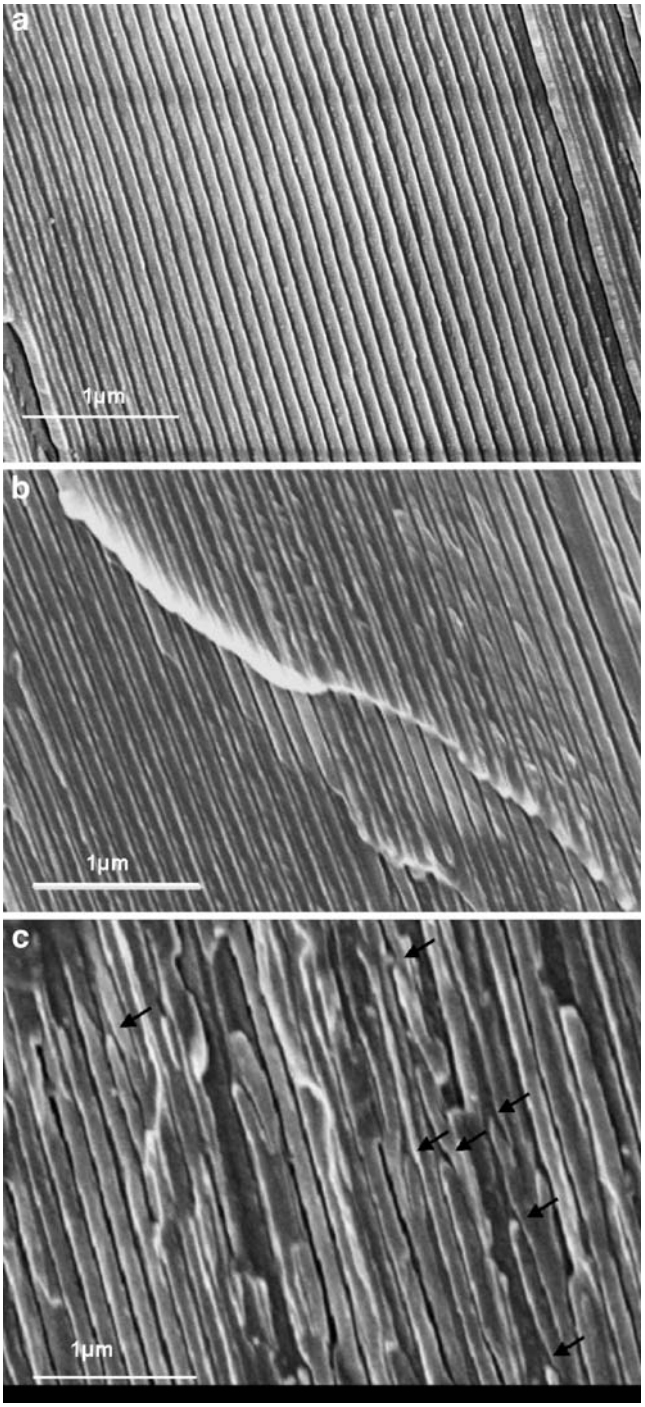

Fig. 11 Typical Cross-sectional FESEM images of anodic alumina after second anodizing at **a** 40 V, **b** 50 V, and **c** 60 V; Set B

Although the troughs would provide seeds for the formation of pores in rows [15], the samples anodized for shorter time did not exhibit any ordered domains (Fig. 3a). The ordering was, however, possible after long time anodizing (Fig. 3b) by self-ordering phenomenon.

Electropolishing was successfully accomplished in Brytal solution as well, although the features were slightly rougher

(deeper) than obtained in Perchloric acid–alcohol solution. This pretreatment resulted in the best pore ordering after anodizing at 50 V (Fig. 7), instead of 40 V. This observation covers uniform pore sizes and shapes, minimum defect density (Fig. 8), and maximum uniformity of the interpore distance or cell size (Fig. 9b) obtained at 50 V. Greater depth of nanopits or troughs after electropolishing in Brytal solution (instead of perchloric acid–alcohol solution) effected an ease in nucleation of the pores, as manifested by an earlier rise in current associated with localized thinning of barrier layer (Fig. 2).

Higher pore density should provide larger effective surface area or smaller barrier layer (or wall) thickness to allow larger nominal current density at a given voltage. The current density of the samples pretreated in Brytal solution during second anodizing was higher at 50 V and above, suggesting a larger pore density in comparison with the samples pretreated in Perchloric acid–alcohol solution. However, this trend was reversed at 40 V. This was accompanied by comparatively improved ordering at 50 V (and above) in case of the samples with prior electropolishing in Brytal solution, while the vice versa was true at 40 V where the ordering was better in case of the sample electropolished in perchloric acid–alcohol solution. These observations reveal that higher pore density during the growth of nanoporous oxide at a given anodizing voltage results in a comparative improvement in ordering.

We consider that difference in density of aluminum and its oxide results in a stress state at the metal–oxide interface. The stress field associated with one pore may overlap with the other neighboring pores. In order to lower the excess strain energy associated with this overlap, the pores tend to remain apart by repelling each other. The smaller the interpore distance, the higher the repulsive force among the pores and better would be the hexagonal ordering.

As far as non-ordering voltages are concerned, it has been noticed by FESEM at high magnification (Fig. 10) that oxide–metal interface at the pore tips (as revealed by dissolution of overlying oxide) is irregular. This seems to be responsible for continual branching (and an accompanied annihilation) of pores at different locations. As a result, the pores do not find sufficient time to interact among themselves through repulsive forces in order to attain an equilibrium hexagonal configuration.

Conclusions

1. This study reveals that different nanoscale morphologies obtained by specific electropolishing pretreatments may have a significant effect on the self-ordering of pores in anodic alumina.
2. The best ordering is obtained at 50 V in 0.3 M oxalic acid at 1 °C when prior electropolishing is performed in Brytal solution, although the best ordering voltage remains the usually known voltage of 40 V after electropolishing in Perchloric acid–alcohol solution.
3. The nanoscale morphology obtained by electropolishing affects the initial stages of anodizing by facilitating the pore nucleation in case of deeper nanopits or troughs. This, in turn, affects the pore density.
4. The higher pore density at a given anodizing voltage improves the self-ordering, which may be attributed to the enhanced repulsive interactions with decrease in interpore spacing or cell size.
5. At non-ordering voltages, pore branching occurs due to irregular shape of the pore tips. This is also accompanied by pore annihilation. These factors do not allow the pore tips to interact with each other for a sufficient time so that they could arrange themselves in a hexagonal pattern.

References

1. Habazaki H, Yamasaki M, Kawashima A, Hashimoto K (2000) Appl Organomet Chem 14:803
2. Mehmood M, Zhang BP, Akiyama E, Habazaki H, Kawashima A, Asami K, Hashimoto K (1998) Corros Sci 40:1
3. Cullis AG, Canham LT, Calcott PDJ (1997) J Appl Phys 82:909
4. Herzer G (1989) IEEE Trans Magn 25:3327
5. Chik H, Xu JM (2004) Mater Sci Eng R-Rep 43:103
6. Alcala G, Mato S, Skeldon P, Thompson GE, Mann AB, Habazaki H, Shimizu K (2003) Surf Coat Technol 173:293
7. Li Y, Shimada H, Sakairi M, Shigyo K, Takahashi H, Seo M (1997) J Electrochem Soc 144:866
8. Schueller GRT, Taylor SR, Hajcsar EE (1992) J Electrochem Soc 139:2799
9. Skeldon P, Shimizu K, Thompson GE, Wood GC (1983) Surf Interface Anal 5:247
10. Keller F, Hunter MS, Robinson DL (1953) J Electrochem Soc 100:411
11. Masuda H, Fukuda K (1995) Science 268:1466
12. Masuda H, Hasegwa F, Ono S (1997) J Electrochem Soc 144:L127
13. Masuda H, Yada K, Osaka A (1998) Jpn J Appl Phys Part 2-Lett 37:L1340
14. Li AP, Muller F, Birner A, Nielsch K, Gosele U (1998) J Appl Phys 84:6023
15. Li FY, Zhang L, Metzger RM (1998) Chem Mat 10:2470
16. Shingubara S, Morimoto K, Sakaue H, Takahagi T (2004) Electrochem Solid State Lett 7:E15
17. Shingubara S, Okino O, Sayama Y, Sakaue H, Takahagi T (1997) Jpn J Appl Phys Part 1-Regul Pap Short Notes Rev Pap 36:7791
18. Asoh H, Nishio K, Nakao M, Tamamura T, Masuda H (2001) J Electrochem Soc 148:B152
19. Kashi MA, Ramazani A (2005) J Phys D-Appl Phys 38:2396
20. Ba L, Li WS (2000) J Phys D-Appl Phys 33:2527
21. Nielsch K, Choi J, Schwirn K, Wehrspohn RB, Gosele U (2002) Nano Lett 2:677
22. Bandyopadhyay S, Miller AE, Chang HC, Banerjee G, Yuzhakov V, Yue DF, Ricker RE, Jones S, Eastman JA, Baugher E, Chandrasekhar M (1996) Nanotechnology 7:360

23. Zhao GY, Xu CL, Guo DJ, Li H, Li HL (2006) J Solid State Electrochem 10:266
24. Nielsch K, Muller F, Li AP, Gosele U (2000) Adv Mater 12:582
25. Liang JY, Chik H, Xu J (2002) IEEE J Sel Top Quantum Electron 8:998
26. Saedi A, Ghorbani M (2005) Mater Chem Phys 91:417
27. Tian YT, Meng GW, Biswas SK, Ajayan PM, Sun SH, Zhang LD (2004) Appl Phys Lett 85:967
28. Kim DK, Tamiya E, Jung KH, Shin HK, Kwon YS (2006) Curr Appl Phys 6:663
29. Martin CR (1994) Science 266:1961
30. Martin CR (1996) Chem Mater 8:1739
31. Gao T, Meng G, Zhang J, Sun S, Zhang L (2002) Appl Phys A-Mater Sci Process 74:403
32. Li J, Papadopoulos C, Xu J (1999) Nature 402:253
33. Mehmood M, Rauf A, Rasheed MA, Saeed S, Akhter JI, Ahmad J, Aslam M (2007) Mater Chem Phys 104:306
34. Masuda H, Yamada H, Satoh M, Asoh H, Nakao M, Tamamura T (1997) Appl Phys Lett 71:2770
35. Liu CY, Datta A, Liu NW, Peng CY, Wang YL (2004) Appl Phys Lett 84:2509
36. Shingubara S, Murakami Y, Morimoto K, Takahagi T (2003) Surf Sci 532:317
37. Ricker RE, Miller AE, Yue DF, Banerjee G, Bandyopadhyay S (1996) J Electron Mater 25:1585
38. Caicedo-Martinez CE, Koroleva EV, Thompson GE, Skeldon P, Shimizu K, Habazaki H, Hoellrigl G (2002) Surf Interface Anal 34:405
39. Konovalov VV, Zangari G, Metzger RM (1999) Chem Mat 11:1949
40. Diggle JW, Downie TC, Goulding CW (1969) Chem Rev 69:365
41. Ono S, Saito M, Asoh H (2004) Electrochem Solid State Lett 7:B21
42. Angelucci R, Corticelli F, Cuffiani M, Dallavalle GM, Malferrari L, Montanari A, Montanari C, Odorici F, Rizzoli R, Summonte C (2003) Nucl Phys B-Proc Suppl 125:164